Received: 16 December 2021 | Revised: 24 May 2022 | Accepted: 25 June 2022

DOI: 10.1002/mp.15865

RESEARCH ARTICLE

MEDICAL PHYSICS

Evaluation of dosimetric effects of metallic artifact reduction and tissue assignment on Monte Carlo dose calculations for ^{125}I prostate implants

Isong Assam[1] | **Javier Vijande**[2,3,4] | **Facundo Ballester**[2,3] | **José Pérez-Calatayud**[5,6] | **Björn Poppe**[7] | **Frank-André Siebert**[1]

[1]UKSH, Campus Kiel, Clinic of Radiotherapy (Radiooncology), Kiel, Germany

[2]Departamento de Física Atómica, Molecular y Nuclear, Universitat de Valencia (UV), Burjassot, Spain

[3]Unidad Mixta de Investigación en Radiofísica e Instrumentación Nuclear en Medicina (IRIMED), Instituto de Investigación Sanitaria La Fe (IIS-La Fe), Universitat de Valencia (UV), Valencia, Spain

[4]Instituto de Física Corpuscular, IFIC (UV-CSIC), Burjassot, Spain

[5]Radiotherapy Department, La Fe Hospital, Valencia, Spain

[6]Radiotherapy Department, Clinica Benidorm, Alicante, Spain

[7]Center for Radiotherapy and Radiation Oncology – University Center for Medical Radiation Physics, Pius-Hospital, Medical Campus of Carl-von-Ossietzky University of Oldenburg, Oldenburg, Germany

Correspondence
Isong Assam, UKSH, Campus Kiel, Clinic of Radiotherapy (Radiooncology), Kiel, Germany.
Email: Isong.Assam@uksh.de

Abstract

Purpose: Monte Carlo (MC) simulation studies, aimed at evaluating the magnitude of tissue heterogeneity in ^{125}I prostate permanent seed implant brachytherapy (BT), customarily use clinical post-implant CT images to generate a virtual representation of a realistic patient model (virtual patient model). Metallic artifact reduction (MAR) techniques and tissue assignment schemes (TAS) are implemented on the post-implant CT images to mollify metallic artifacts due to BT seeds and to assign tissue types to the voxels corresponding to the bright seed spots and streaking artifacts, respectively. The objective of this study is to assess the combined influence of MAR and TAS on MC absorbed dose calculations in post-implant CT-based phantoms. The virtual patient models used for ^{125}I prostate implant MC absorbed dose calculations in this study are derived from the CT images of an external radiotherapy prostate patient without BT seeds and prostatic calcifications, thus averting the need to implement MAR and TAS.

Methods: The geometry of the IsoSeed I25.S17plus source is validated by comparing the MC calculated results of the TG-43 parameters for the line source approximation with the TG-43U1S2 consensus data. Four MC absorbed dose calculations are performed in two virtual patient models using the *egs_brachy* MC code: (1) TG-43-based $D_{w,w\text{-}TG43}$, (2) $D_{w,w\text{-}MBDC}$ that accounts for interseed scattering and attenuation (ISA), (3) $D_{m,m}$ that examines ISA and tissue heterogeneity by scoring absorbed dose in tissue, and (4) $D_{w,m}$ that unlike $D_{m,m}$ scores absorbed dose in water. The MC absorbed doses (1) and (2) are simulated in a TG-43 patient phantom derived by assigning the densities of every voxel to 1.00 g cm^{-3} (water), whereas MC absorbed doses (3) and (4) are scored in the TG-186 patient phantom generated by mapping the mass density of each voxel to tissue according to a CT calibration curve. The MC absorbed doses calculated in this study are compared with VariSeed v8.0 calculated absorbed doses. To evaluate the dosimetric effect of MAR and TAS, the MC absorbed doses of this work (independent of MAR and TAS) are compared to the MC absorbed doses of different ^{125}I source models from previous studies that were calculated with different MC codes using post-implant CT-based phantoms generated by implementing MAR and TAS on post-implant CT images.

Results: The very good agreement of TG-43 parameters of this study and the published consensus data within 3% validates the geometry of the IsoSeed I25.S17plus source. For the clinical studies, the TG-43-based calculations show a D_{90} overestimation of more than 4% compared to the more realistic MC methods due to ISA and tissue composition. The results of this work generally show few discrepancies with the post-implant CT-based dosimetry studies with respect to the D_{90} absorbed dose metric parameter. These discrepancies are mainly Type B uncertainties due to the different ^{125}I source models and MC codes.

Conclusions: The implementation of MAR and TAS on post-implant CT images have no dosimetric effect on the ^{125}I prostate MC absorbed dose calculation in post-implant CT-based phantoms.

KEYWORDS

metallic artifact reduction, Monte Carlo dosimetry, post-implant CT, prostate brachytherapy, tissue assignment schemes, voxelized virtual patient model

1 | INTRODUCTION

In low dose rate (LDR) brachytherapy (BT), radioactive seeds of short-lived, low-energy photon emitters, such as ^{125}I and ^{103}Pd, are permanently implanted into the prostate gland using transrectal ultrasound guidance. This procedure has gained wide acceptance for the treatment of early stage prostate cancer, in which the tumor is within or near the prostate gland.[1]

Most commercial LDR BT treatment planning systems (TPSs) use the TG-43 absorbed dose calculation formalism based on the isotropic point or line source model. In this formalism, absorbed dose at a point in water is calculated as the superposition of the absorbed dose of each seed at the point, assuming that radiation from each seed is unaffected by the presence of the other seeds.[1] Thus, the TG-43 formalism ignores tissue heterogeneity and interseed scattering and attenuation (ISA), resulting in an overestimation of the total absorbed dose delivered to the patient.[2–6]

The TG-186 report provides recommendations for model-based dose calculation algorithms (MBDCA) aimed at resolving the shortcomings of the TG-43 formalism.[3] MBDCA offers the possibility of modeling radiation transport in non-water media and considering ISA, resulting in a more accurate calculation of the total absorbed dose actually delivered to the patient.[3] MBDCA such as Monte Carlo (MC) methods generally compute absorbed dose by assigning interaction cross sections on a voxel-by-voxel basis, hence the need to develop a virtual representation of a realistic patient model (virtual patient model). The virtual patient-specific model can be derived from the patient's CT scans by assigning CT numbers to tissue types.[3,4,7,8] MC studies aimed at evaluating the magnitude of ISA, and tissue compositions in permanent seed implant BT customarily use clinical post-implant CT images to generate voxelized virtual patient models.

Metallic artifact reduction (MAR) techniques and tissue assignment schemes (TAS) are applied to the post-implant CT images to mitigate metallic artifacts due to BT seeds and to assign tissue types to the voxels corresponding to the bright seed spots and streaking artifacts, respectively. Miksys et al. investigated four MAR techniques on post-implant prostate BT–CT images and reported the inability of all four MAR techniques studied to completely eradicate artifacts, and the interdependence of MAR method and TAS.[7] These findings may have significant effects on the calculated absorbed dose because photoelectric effect, the cross section of which is proportional to the fourth power of the atomic number (Z) of the medium, is the predominant mode of interaction at low photon energies. Implementing MAR and TAS on post-implant CT data results in differences between the post-MAR CT numbers and the actual CT numbers, assuming that the patients' CT images were acquired before BT seeds implantation.

The objective of this study is to assess the dosimetric effects of MAR and TAS on the MC absorbed dose calculations in post-implant CT-based phantoms for ^{125}I permanent prostate implant. The voxelized virtual patient models used for the ^{125}I permanent implant prostate BT MC absorbed dose calculations in this study are derived from the CT images of an external radiotherapy prostate patient without BT seeds and prostatic calcifications, thus avoiding the need to implement MAR and TAS. Post-implant CT-based phantoms are generated by implanting MAR and TAS on post-implant CT images.

Four MC absorbed doses, $D_{w,w\text{-}TG43}$, $D_{w,w\text{-}MBDC}$, $D_{m,m}$, and $D_{w,m}$, are calculated using the EGSnrc[9] MC application *egs_brachy*.[10] Absorbed dose is also calculated with the TG-43 formalism–based commercial TPS VariSeed v8.0 (Varian Medical Systems, Inc., Palo Alto, CA). An absorbed dose profile analysis of a line through the prostate and gamma index (γ index) methods[11] is

used to evaluate the agreement between the TPS- and MC absorbed dose distributions. The TPS- and MC absorbed doses are compared using dose–volume histogram (DVH) dosimetry parameters D_{50}, D_{90}, D_{98}, V_{75}, V_{100}, and V_{150} for the prostate as the planning target volume (PTV) as well as D_{10} and D_{2cc} for the urethra and rectum, respectively, as organs at risk (OARs). To evaluate the dosimetric effect of MAR and TAS, the MC absorbed doses calculated in this work are compared to post-implant CT-based dosimetry calculations of different ^{125}I source models and MC codes from previous studies.

2 | MATERIALS AND METHODS

2.1 | Brachytherapy source geometry

The I25.S17plus ^{125}I BT seed manufactured by Eckert & Ziegler BEBIG (Berlin, Germany) is used here as a loosed BT source. The modeled I25.S17plus source geometry is directly taken from previous studies.[12–14] The I25.S17plus is made up of a 0.055-mm thick titanium grade 2 tube (percentage elemental composition: 0.015% H, 0.1% C, 0.03% N, 0.25% O, 0.2% Fe, 99.405% Ti) with a density of 4.512 g cm^{-3} encapsulating the source element. The source element consists of a cylindrical silver rod of density 10.5 g cm^{-3} with an outer diameter of 0.51 mm and a length of 3.40 mm. The silver rod is coated with a radioactive silver iodide layer of thickness 1.0 μm and density of 5.675 g cm^{-3}, giving the source an active length of 3.40 mm. The titanium encapsulation is sealed via laser welding using two hemispherical end caps with an end-weld thickness 0.4 mm each. The I25.S17plus seed has a total length and outer diameter of 4.5 and 0.80 mm, respectively.

2.2 | Monte Carlo simulation

2.2.1 | MC code description

This study uses the EGSnrc application *egs_brachy* v2017.09.15, a versatile and fast MC code designed specifically for BT applications.[10] Detailed descriptions of the *egs_brachy* MC code can be found in the study of Chamberland et al.[10] and the *egs_brachy* user manual.[15] The *egs_brachy* MC application has also been benchmarked and validated against the extensively used BT MC code BrachyDOSE.[10,16,17] The Type B uncertainties of *egs_brachy* are recently compared to other state-of-the-art BT MC codes, PENELOPE-2018, and MCNP.[18]

egs_brachy utilizes the modern and actively maintained EGSnrc C^{++} class library[19] (called egs^{++}) for modeling geometries and particle sources. In addition, *egs_brachy* also led to several enhancements to the general-purpose egs^{++} library in the form of new geometry and shape classes.[10,19] This study utilizes the reference features of the *egs_brachy* MC code without modification.

2.2.2 | MC absorbed dose calculation

Particles are initialized within the source using the ^{125}I-energy spectrum from the NCRP Report 58.[20] The photon cutoff energy of 1 keV is used in all calculations except for the air-kerma strength simulation that uses an energy cutoff of 5 keV to suppress the 4.5 keV characteristic X-rays emanating from the titanium encapsulation as recommended.[1] Electron transport is not modeled due to the negligible range of the secondary electrons produced by the relatively low-energy photons emitted from the BT source. This study also utilizes particle recycling; a variance reduction technique that reuses particles escaping from the source geometry an arbitrary number of times thus increasing the efficiency of the simulation.[15] Photons emitted from the source are recycled once, and each emitted photon is rotated by an arbitrary angle about the active length of the source (z-axis) prior to being recycled. Simulations that applied particle recycling are checked to ensure that the recycled particles do not result in nonindependent events and correlated data.

Photon cross sections and the distributed mass-energy absorption coefficients for the various media are taken from the XCOM data set.[21] Compton scattering is treated with the impulse approximation model, whereas bremsstrahlung cross sections are modeled with the NRC library, which is a version of the NIST database with corrected electron–electron bremsstrahlung contributions. Kawrakow's theory[22] is used to derive electron impact ionization cross sections. Photoelectric absorption, Rayleigh scattering, and fluorescent emission of characteristic X-ray after photoelectric absorption are also explicitly modeled in each simulation. Due to the negligible range of the secondary electrons produce by ^{125}I, the absorbed dose in the medium is approximated as collision kerma using the track length kerma estimator.

The general two-dimensional (2D) line source approximation[1] is used and the absorbed dose is outputted in Gy per effective number of histories. The MC absorbed dose (D_{MC}) is converted into total absorbed dose D_{tot} in Gy using the following equation:

$$D_{tot} = S_{K,ref} \cdot \frac{D_{MC}}{S_K^{hist}} \cdot \int_0^{t_{end}} e^{-\lambda t} \quad (1)$$

where $S_{K,ref}$ is the air-kerma strength of the source provided by the manufacturer in U (1 U = 1 μGy M^2 h^{-1}); S_K^{hist} is the air-kerma strength per history calculated by

egs_brachy in Gy cm^2/history, whereas $t = 0$ and $t = t_{end}$ are the treatment start and end times, respectively; and λ is the radionuclide's decay constant. For a permanent implant, taking $t_{end} \rightarrow \infty$

$$D_{tot} = S_{K,ref} \cdot \frac{D_{MC}}{S_K^{hist}} \cdot \tau \quad (2)$$

where τ (h) is the mean lifetime of the radionuclide $(1/\lambda)$.[15]

When a voxel in a scoring phantom is partially occupied by a seed, an MC voxel–volume correction technique is used to subtract the volume of the seed from the phantom's voxel. For accurate absorbed dose calculation, energy deposition is only scored in the portion of the voxel unoccupied by the seed.[15]

2.2.3 | Source geometry validation

The geometry of the modeled IsoSeed I25.S17plus line source is benchmarked by comparing the MC-calculated results of the 2D TG-43 parameters with published consensus values in the TG-43U1S2 report.[23] The simulations of the TG-43 dosimetry parameters are done according to Taylor et al.[16] The NIST WAFAC primary collimator with a diameter of 8 cm located 30 cm from the source subtends a circle with a diameter of ~2.7 cm located 10 cm from the source. The air-kerma strength per history is scored in vacuo in rectilinear voxels of thickness 0.05 cm with a voxel's face of area 2.7×2.7 cm^2 centered on the transverse axis at a distance of 10 cm from the source. The large voxel size of $2.7 \times 2.7 \times 0.05$ cm^3 averages the air-kerma strength per history over a region covering approximately the solid angle subtended by the NIST WAFAC primary collimator.[16]

To calculate other TG-43 parameters, absorbed dose rates are scored by aligning the source along the *z*-axis of a cylindrical water phantom with a radius and height of 15 and 30 cm, respectively. To minimize the impact of the volume size effect, the following voxel sizes are used with respect to the radial distance (r) from the cylinder's axis; 0.01 cm^3 for $r \leq 1$ cm, 0.05 cm^3 for 1 cm $< r \leq 5$ cm, and 0.1 cm^3 for 5 cm $< r \leq 10$ cm.[16] The dose-rate constant is the quotient of dose at reference point and the air-kerma strength per history. Enough histories (about 2×10^{10}) are simulated to ensure the statistical component of uncertainty in the area of interest is below 1% in all simulations.

2.2.4 | Virtual patient models

The voxelized virtual patient model enables MC absorbed dose calculation in phantoms that are derived from the patient's DICOM CT data sets. The virtual patient models of this study are generated by assigning the mass density to the CT number of the tissue on a voxel-by-voxel basis using a CT calibration curve.

TABLE 1 Mean CT number versus mass density calibration for the SOMATOM Sensation CT scanner

Tissue equivalent inserts	Mean CT number (HU)	Mass density (g cm^{-3})
Lung (inhale)	−795.94	0.20
Lung (exhale)	−505.44	0.50
Adipose	−64.56	0.96
Breast (50/50)	−33.38	0.99
Water	5.19	1
Plastic water	12.56	1.029
Muscle	40.50	1.06
Liver	66.56	1.07
Trabecular bone (200 mg cm^{-3})	237.75	1.16
Dense bone (800 mg cm^{-3})	923.50	1.53
Core bone (1750 mg)	1487	2.15
Titanium	3070	4.51

Abbreviation: HU, Hounsfield unit.

An electron density phantom, model 062M (CIRS, Virginia, USA) with its corresponding set of tissue equivalent electron density insets, is used to calibrate the CT number to mass density of the CT scanner. The electron density phantom is scanned by a SOMATOM Sensation CT scanner (Siemens Medical Solution, Erlangen, Germany) with the same scan protocol used for external radiotherapy and post-implant prostate BT patients. The Hounsfield unit (HU) versus mass density calibration curve is derived by drawing ROIs over each tissue-equivalent electron density insert and recording the corresponding mean HU. Table 1 shows the CT scanner's calibration of HU versus mass density. The CT calibration curve in this study is in good agreement with the CT calibration curve derived from the SOMATOM Emotion CT scanner (Siemens Medical Solution, Erlangen, Germany), as discussed in Miksys et al.[7]

The CT images of an external radiotherapy prostate patient without implanted ^{125}I BT seeds and prostatic calcifications are used to generate two virtual patient models: the TG-43 and TG-186 patient phantoms. CT images without BT seeds avert the need to implement MAR and TAS around the seeds, since there are no bright seed spots and streaking artifacts compared to post-implant CT images of permanent prostate implant patients.

The EGSnrc application *ctcreate* is used to create the two patient phantoms from the patient's DICOM CT images by converting the CT data to materials and

densities for each voxel according to the CT calibration curve.[24] The TG-43 patient phantom is derived by overwriting the CT numbers of all voxels to the reference medium, water (1.00 g cm^{-3}), thus ignoring the effect of tissue heterogeneity.[1] The TG-186 patient phantom is obtained by assigning one of the four tissues, namely, prostate, rectum, mean adipose, and cortical bone to each voxel using the CT calibration curve. The body tissue compositions of the TG-186 patient phantom are taken from TG-186 and ICRU 46 reports[3,25] in accordance with TG-186 recommendation.[3]

2.2.5 | Clinical data study

The CT images of the external radiotherapy prostate patient without ^{125}I BT seeds implants and prostatic calcification are imported into VariSeed TPS, and the prostate, urethra, bladder, and rectum contours are delineated. Urethra segmentation is used to contour the urethra. Although it is difficult to delineate the absolute position of the urethra in CT without catheter in place, the differences in absorbed dose calculations are more important than the absolute position of the urethra in this study. Overall, 41 loosed IsoSeed I25.S17plus seeds with reference air-kerma strength (S_K) of 0.635 U per seed are virtually implanted into the prostate volume of 28.37 cm^3 with a prescription dose of 145 Gy. The implantation is aimed at meeting the following dosimetry constrains: $D_{90} > 100\%$ of prescription dose, $V_{100} \geq 95\%$ of PTV, and $V_{150} \leq 50\%$ of PTV. D_{90} is the dose that covers 90% of the PTV, and V_{100} is the percentage of the PTV, which receives 100% of the prescription dose of 145 Gy. For the OARs, the rectum's $D_{2cc} \leq$ prescription dose and the urethra's $D_{10} < 150\%$ of the prescription dose, where D_{2cc} is the dose that covers a volume of 2 cm^3 of the rectum. The dosimetry constrains are in conformity with ESTRO/EAU/EORTC prostate BT guidelines.[26] The TG-43 and TG-186 patient phantoms created from the CT data set with voxel sizes; $0.13 \times 0.13 \times 0.30$ cm^3 are resampled to match the VariSeed dose grid resolution of $0.10 \times 0.10 \times 0.30$ cm^3. As voxels far away from the PTV receive very little or no doses, both phantoms are cropped to a few centimeters around the right and left femoral heads leaving the prostate, bladder, and rectum for faster simulation as shown in Figure 2.

Seed positions exported from the VariSeed treatment plan are used to implant seeds perpendicularly to the transverse plane of both the TG-43 and TG-186 patient phantoms. The following MC absorbed doses are calculated following the specifications described in Section 2.2.2:

1. $D_{w,w\text{-}TG43}$: A mock-up of TG-43 calculations where absorbed dose is scored in the TG-43 patient phantom by the superposition of single-source absorbed dose-to-water, thus eliminating ISA and tissue heterogeneity.[1]
2. $D_{w,w\text{-}MBDC}$: Absorbed dose is scored in the TG-43 patient phantom to disregard the effect of tissue composition while accounting for ISA.[3]
3. $D_{m,m}$: Particles are transported in tissues of the TG-186 patient phantom accounting for both ISA and tissue heterogeneity, and absorbed dose is scored in tissue.
4. $D_{w,m}$: Particles are transported in tissues of the TG-186 patient phantom accounting for both ISA and tissue heterogeneity but absorbed dose is scored in water in accordance to TG-186 convention.[3]

The VariSeed-exported DICOM RT (absorbed dose, structures) data set and the four MC calculated absorbed doses are imported into the Computational Environment for Radiological Research software[27] for cumulative DVHs computation, dose–line profile and gamma index analyses. Before calculating the DVHs, an upper cutoff absorbed dose of 500 Gy is applied to the TPS and the four MC calculated absorbed doses in order to remove the extremely high absorbed doses at the seeds' center, which are clinically irrelevant. The voxel sampling size used for the DVHs calculation is the same as the dose grid resolution (0.1 cm). The dosimetry parameters extracted from the DVH for the TPS and MC dosimetry comparison include D_{50}, D_{90}, D_{98}, V_{75}, V_{100}, and V_{150} for the prostate as well as D_{10} and D_{2cc} for the urethra and rectum, respectively. The relative percentage differences of the absorbed dose (ΔD_x) and volume (ΔV_x) between two absorbed dose computation methods A and B are calculated from Equations (3) and (4), respectively. The results of both ΔD_x and ΔV_x are presented in the tables as percentage difference, Δ *Method A, Method B*:

$$\Delta D_x = \frac{D_x^A - D_x^B}{D_x^A} \cdot 100 \quad (3)$$

$$\Delta V_x = \frac{V_x^A - V_x^B}{V_x^A} \cdot 100 \quad (4)$$

As the DVHs do not display spatial information, a dose profile analysis of a line through the prostate and the gamma index (γ index) technique[11] are used as additional absorbed dose comparison criteria to evaluate the agreement of the four MC ($D_{w,w\text{-}TG43}$, $D_{w,w\text{-}MBDC}$, $D_{m,m}$, and $D_{w,m}$) and TPS calculated absorbed dose distributions. The gamma criteria used in this study are 2%/2 mm and a 5% low dose threshold with an acceptable gamma pass rates of over 90% for each absorbed dose calculation. The stricter 2%/2 mm gamma criterion is used, as opposed to the 3%/3 mm recommended by AAPM TG-119,[28] due to the high-dose gradients encountered in BT as proposed by some

researchers.[29–31] Absorbed dose comparison among the various MC simulations aimed at quantifying the effect of ISA ($D_{ww\text{-}TG43}$ vs. $D_{w,w\text{-}MBDC}$), tissue composition ($D_{w,w\text{-}MBDC}$ vs. $D_{m,m}$), and the combined effect of ISA and tissue composition ($D_{ww\text{-}TG43}$ vs. $D_{m,m}$) are also calculated using Equations (3) and (4). The clinical TG-43 MC simulation, $D_{w,w\text{-}TG43}$, is used instead of the TPS in order to eliminate small differences in the TG-43 parameter results of this study and consensus data due to differences in MC transport codes. VariSeed uses the consensus data in routine clinical treatment planning.

The calculated MC absorbed doses in this study are verified by comparing them with published MC absorbed doses scored in homogeneous water or prostate tissue phantoms using different ^{125}I source models and MC codes.[2,5,6] These tissue phantoms are not CT-based and are generated by overwriting all voxels to water or prostate tissue. The tissue phantoms are therefore independent of MAR and TAS.

To evaluate the dosimetric effect of MAR and TAS, the MC absorbed doses of this work are compared to post-implant CT-based dosimetry calculations of different ^{125}I source models and MC codes from previous MC studies.[5,8] The post-implant CT-based phantoms were derived by applying MAR and TAS on post-implant CT images, and tissues types are assigned to the voxelized patient virtual phantoms using organ-specific material assignment or a CT calibration curve.

3 | RESULTS AND DISCUSSIONS

3.1 | Source geometry and TG-43 parameters verification

The comparison between the TG-43 parameter results calculated in this study and published consensus values[23] are shown in the Supporting Information section.

3.1.1 | Dose-rate constant and radial dose function

The dose-rate constant of the NIST WAFAC (Λ_{WAFAC}) and line-source radial dose function ($g_L(r)$) results of this study and consensus are in very good agreement within 1.6% and 0.5%, respectively (Tables S1 and S2).

3.1.2 | 2D anisotropy function $F(r,\theta)$ and along–away dose rates

The 2D anisotropy function results of this study ($_{MC}F(r, \theta)$) and the consensus ($_{CON}F(r, \theta)$) show relative differences of up to 9.0% at r = 0.25 cm and angles less than 15° (Table S3a). Further comparison between the 2D anisotropy function results of this study and the values reported by Carleton Laboratory for Radiotherapy Physics (CLRP) TG-43 parameter database for BT, version 2 ($_{CLRP}F(r, \theta)$)[14,17] at r = 0.25 cm, agrees with a maximum difference of 1.0% at θ = 0° (Table S3a). As this study and CLRP used the same version of the *egs_brachy* MC code, the high disparity between this study and the consensus is due to the larger Type B uncertainties between MCNP5 v.1.6 (consensus) and *egs_brachy* MC transport codes, especially when simulating doses in voxels that are very close to the seed center.[18] The 2D anisotropy function results at r = 0.25 cm of all three simulations are depicted in Figure 1.

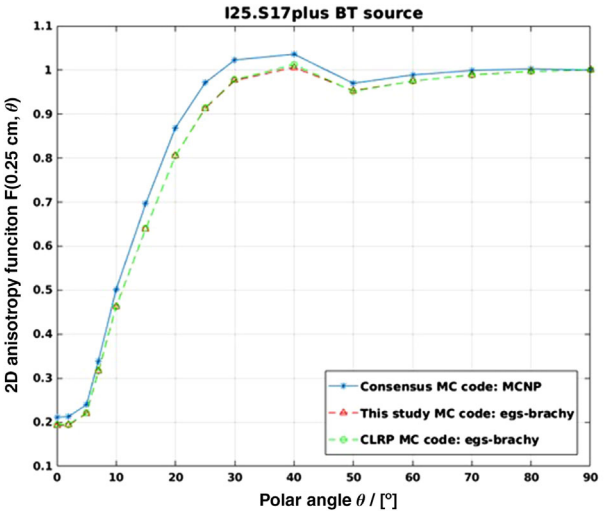

FIGURE 1 Two-dimensional (2D) anisotropy function, $F(0.25\ cm, \theta)$ values comparison from this study, the Carleton Laboratory for Radiotherapy Physics (CLRP) TG-43 parameter database, and the consensus

The 2D anisotropy function results comparison of this study with the consensus dataset show low relative differences of up to 3.8% at the reference distance (r = 1 cm) and a very good agreement within 1.9% at larger distances (Table S3b).

The calculated dose-rate per unit source strengths (cGy h^{-1} U^{-1}) at distances along the source long axis and away from the source axis of symmetry are shown in the along–away format in Table S4. This study and the consensus data agree within 3.9% for distances less than 6 cm along the source. The maximum uncertainty of 5.3% is recorded at distances 7 and 4 cm along and away from the seed center, respectively. The very good agreement of TG-43 parameters of this study and the published consensus data validates the geometry of the IsoSeed I25.S17plus source.

3.2 | Clinical data studies

The transverse views of the TG-43 and TG-186 patient phantoms generated from CT slice 12 are shown in

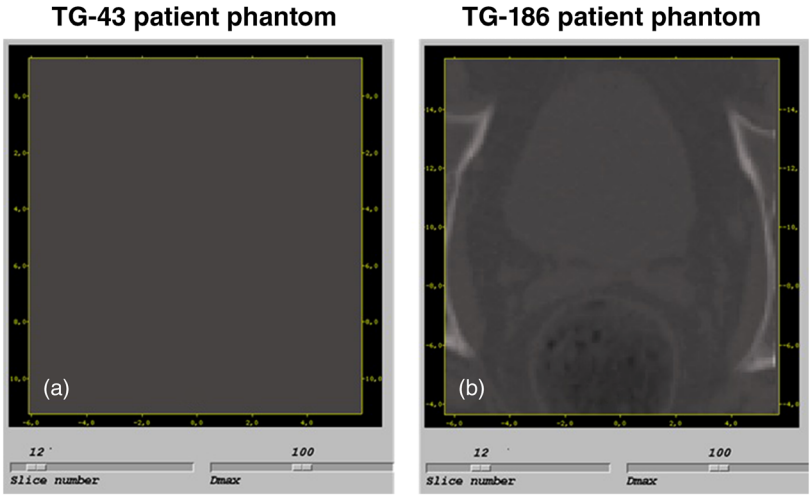

FIGURE 2 The transverse view of the TG-43 (a) and TG-186 (b) patient phantoms generated from CT slice 12. Images are generated using the *dosxyz_show* application of EGSnrc.

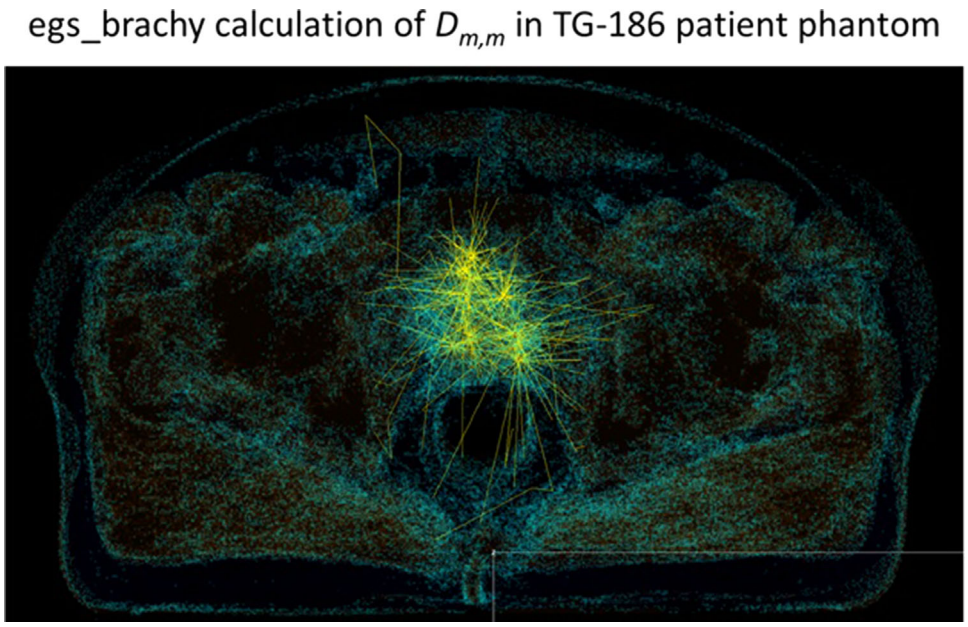

FIGURE 3 Prostate, rectum, mean adipose, and cortical bone tissues and particle tracks visualization of $D_{m,m}$ simulation with the TG-186 patient phantom. Image is generated using the *egs_view* application of EGSnrc.

Figure 2a,b, respectively. The TG-43 patient phantom is a homogeneous water tissue, whereas the TG-186 patient phantom consists of prostate, rectum, mean adipose, and cortical bone tissues assigned to each voxel using the CT calibration curve.

Figure 3 shows a subset of the $D_{m,m}$ calculation displaying tissues and photon tracks (yellow lines) of photons emitted from the ^{125}I seeds, which are virtually implanted in the prostate of the TG-186 patient phantom. Up to 10^6 histories are used in this simulation to visually verify that the seeds are confined in the prostate; before starting the TG-43 calculations in the TG-43 patient phantom which is a cube of water (Figure 2a). The extend of the particle tracks also motivated the cropping of both patient phantoms to a few centimeters around the right and left femoral heads for faster simulation as stated in Section 2.2.5 (Figure 2b).

The TPS- and MC ($D_{w,w\text{-}TG43}$, $D_{w,w\text{-}MBDC}$, $D_{m,m}$, and $D_{w,m}$) calculated DVHs with an absorbed dose cutoff of 500 Gy for the prostate, urethra, bladder, and rectum are shown in Figure 4.

3.2.1 | Dose–line profiles and gamma index analyses

Figure 5a shows the line AB through the prostate with a high-density material, the pubis bone at B. The

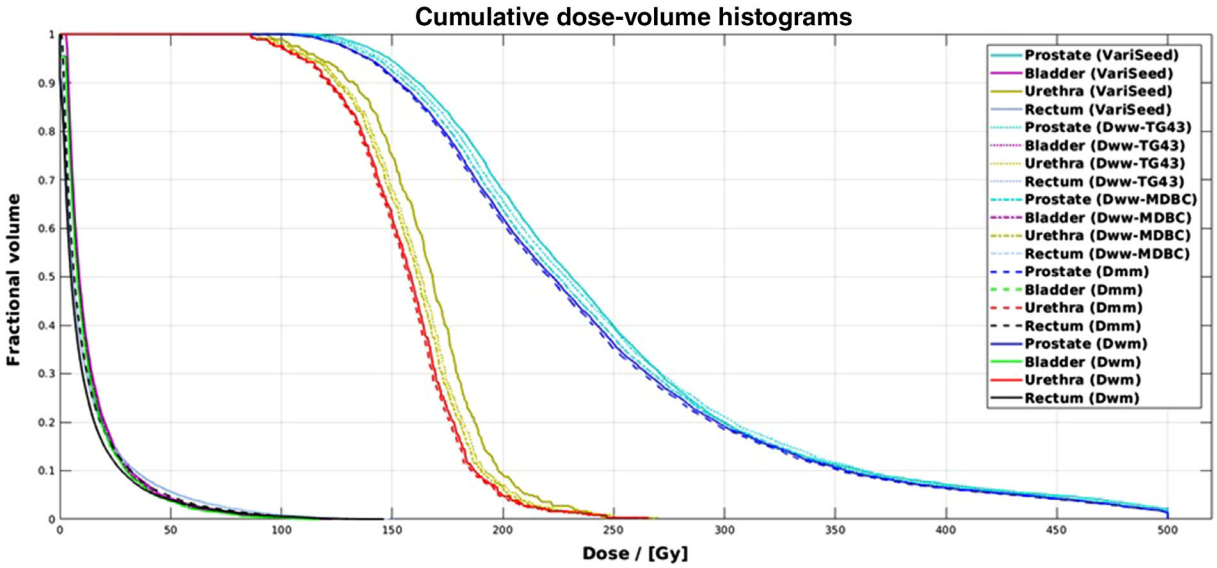

FIGURE 4 Dose–volume histograms (DVHs) with a cutoff absorbed dose of 500 Gy for the prostate, urethra, bladder and rectum of VariSeed treatment planning system (TPS), and Monte Carlo (MC) absorbed dose calculation methods; $D_{w,w\text{-}TG43}$, $D_{w,w\text{-}MBDC}$, $D_{m,m}$, and $D_{w,m}$

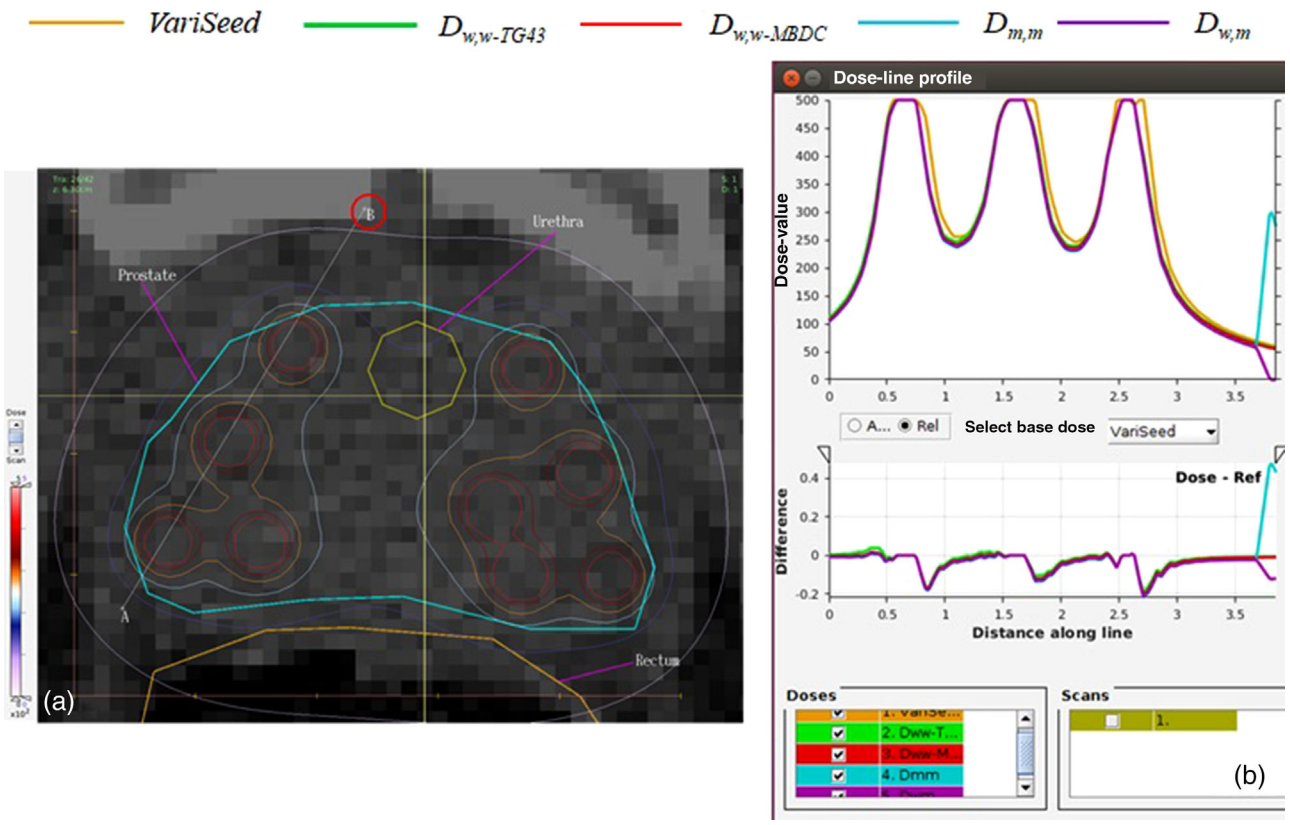

FIGURE 5 (a) The line AB through the prostate with a high-density material, the pubis bone at B. (b) Dose profile comparison among VariSeed, $D_{w,w\text{-}TG43}$, $D_{w,w\text{-}MBDC}$, $D_{m,m}$, and $D_{w,m}$ calculated absorbed doses along the line AB with an upper absorbed dose cutoff of 500 Gy

corresponding dose–line profiles of VariSeed and MC calculations ($D_{w,w\text{-}TG43}$, $D_{w,w\text{-}MBDC}$, $D_{m,m}$, and $D_{w,m}$) in the voxels along the line AB with an upper cutoff absorbed dose of 500 Gy are depicted in Figure 5b.

The three peaks in Figure 5b are the centers of the three seeds along the line AB in Figure 5a. The position of the peaks of all the dose profiles along the line AB are within a tenth of mm apart from each other, hence

TABLE 2 The relative dose differences between VariSeed and the respective Monte Carlo (MC) absorbed dose calculations for the prostate, urethra, and rectum

Structure	DVH parameter	Calculated DVH parameter values					Relative difference from TPS (%)			
		VariSeed (TPS)	$D_{w,w\text{-}TG43}$	$D_{w,w\text{-}MBDC}$	$D_{m,m}$	$D_{w,m}$	$D_{w,w\text{-}TG43}$	$D_{w,w\text{-}MBDC}$	$D_{m,m}$	$D_{w,m}$
Prostate	D_{50} (Gy)	230.7	228.3	225.1	220.8	222.5	1.0	2.4	4.3	3.6
	D_{90} (Gy)	162.0	158.7	155.9	152.2	153.2	2.0	3.8	6.0	5.4
	D_{98} (Gy)	134.9	131.6	129.0	125.3	125.7	2.4	4.4	7.1	6.8
	V_{75} (%)	99.98	99.97	99.91	99.66	99.68	0.0	0.1	0.3	0.3
	V_{100} (%)	95.93	94.87	94.39	92.94	93.28	1.1	1.6	3.1	2.8
	V_{150} (%)	56.81	55.22	53.50	51.41	52.17	2.8	5.8	9.5	8.2
Urethra	D_{10} (Gy)	198.1	192.0	190.3	186.0	187.4	3.1	3.9	6.1	5.4
Rectum	D_{2cc} (Gy)	101.5	94.05	92.55	86.05	83.05	7.3	8.8	15.2	18.2

Abbreviations: DVH, dose–volume histogram; TPS, treatment planning system.

substantiating that there are no seed positioning errors between VariSeed and the MC simulations. The similar shapes of the dose profiles also certify the integrity of the MC simulations with respect to the TPS. The dose profiles are not exactly superimposed on each other due to their respective small absorbed dose differences. The relative absorbed dose differences between the respective MC and VariSeed calculated values along the line AB for this CT slice (26) are within ±5% in the prostate and −20% in the regions immediately after the center of the seed as displayed below the dose line profiles. The negative values of the absorbed dose difference close to the seeds' center imply that TPS absorbed doses are higher than the MC absorbed doses. The absorbed dose differences are largely due to the high relative differences in the 2D anisotropy function close to the source center, $F(0.25\ cm, \theta)$ between this study and consensus as depicted in Figure 1.

The $D_{m,m}$ dose profile shows a spontaneous increase at the end of the line (B) compared to the other absorbed doses. This sharp increase in $D_{m,m}$ is due to the presence of the pubis bone at B. The more than 40% increase in $D_{m,m}$ at B relative to VariSeed (reference medium) is due to the mass-energy absorption coefficients dependence on tissue composition, which is most significant for photons at low energies below 50 keV.[3] The fact that VariSeed, $D_{w,w\text{-}TG43}$, and $D_{w,w\text{-}MBDC}$ dose profiles are invariant at B also validates the veracity of the MC code.

The γ index comparison of the MC-simulated absorbed dose distributions of the prostate with respect to the TPS gives the following results: the gamma pass rates for $D_{w,w\text{-}TG43}$ and $D_{w,w\text{-}MBDC}$ absorbed dose distributions are 95.95% and 95.80%, respectively, whereas the MC calculations where particles are transported in tissues have the gamma pass rates of 95.31% and 95.78% for $D_{m,m}$ and $D_{w,m}$ absorbed dose distributions, respectively. The γ index global results for the 2%/2-mm gamma criterion are clearly above the acceptable gamma pass rates of over 90% for each absorbed dose calculation,[28–31] thus confirming the prostate absorbed dose homogeneity of the MC calculations relative to the TPS.

3.2.2 | Superposition calculations

Both VariSeed and $D_{w,w\text{-}TG43}$ MC calculations are based on the TG-43 dosimetry formalism, which is the superposition of single-source absorbed dose-to-water, thus eliminating ISA and tissue heterogeneity.[1] The superposition calculations are thus independent of MAR and TAS. The results of the superposition calculations for the prostate prescription dose of 145 Gy are presented in Table 2.

The VariSeed calculated absorbed dose metrics are slightly higher than their $D_{w,w\text{-}TG43}$ counterpart. The TPS and MC superposition calculation ($D_{w,w\text{-}TG43}$) generally agree within 2.8% (V_{150}) for the prostate with the maximum relative difference of 7.3% for the rectum's D_{2cc} dose. The small relative differences between VariSeed and $D_{w,w\text{-}TG43}$ MC absorbed dose metrics reported in this study are because VariSeed uses the consensus data in routine clinical treatment planning instead of the *egs_brachy* calculated TG-43 parameters. The rectum's D_{2cc} relative difference of 7.3% is partly due to along–away dose rates deviations at distances above 3 cm from the source (Table S4) and because less particles transverse the rectum, hence larger Type A uncertainties.

To verify the MC absorbed doses calculated in this study, the MC absorbed doses are compared with MC absorbed doses from previous studies scored in homogeneous tissue phantoms using different ^{125}I sources and MC codes. The tissue phantoms consist of either water or prostate tissue and are independent of MAR and TAS. The MC absorbed dose verification results are shown in Table 3. The 2.4% relative deviation for D_{98} of this study concurs with previous studies by Mason et al.[32,33] who reported a maximum difference of 3.7%

TABLE 3 Comparison between the Monte Carlo (MC) absorbed dose scored in homogeneous tissue phantoms in this study and published results from previous studies using different ^{125}I sources and MC codes

	Study	MC code	^{125}I source model	Compared MC doses	Relative difference of DVH parameters (%)					
					D_{90}	D_{98}	V_{100}	V_{150}	D_{10}	D_{2cc}
TG-43 formalism with TPS	This study	*egs_brachy* v2017.09.15	I25.S17plus	VariSeed vs. $D_{w,w\text{-}TG43}$	2.0	2.4	1.1	2.8	3.1	7.3
	Mason et al.[33]	MCNPX v2.5.0	Model 6711	VariSeed vs. MC-SUP	3.3	3.7	1.5	5.6	1.8	2.2
	Landry et al.[5]	GEANT4 v.9.3	Model 2301	VariSeed vs. $D_{TG\text{-}43}$	2.0					
	Carrier et al.[6]	GEANT4 v.8.0	SelectSeed	*Clinical* vs. *NoSeedMC*	0.0		0.0			
ISA	This study	*egs_brachy* v2017.09.15	I25.S17plus	$D_{w,w\text{-}TG43}$ vs. $D_{w,w\text{-}MBDC}$	1.8	2.0	0.51	3.1	0.89	1.6
	Chibani et al.[2]	MCNP v.5	I25.S06	LSKS vs. FMCS	2.0–5.0		0.41	5.2		
	Carrier et al.[6]	GEANT4 v.8.0	SelectSeed	*NoSeedMC* vs. *WaterMC*	4.0		1.1			
Tissue effect	This study	*egs_brachy* v2017.09.15	I25.S17plus	$D_{w,w\text{-}MBDC}$ vs. $D_{m,m}$	2.4		1.5			
	Carrier et al.[6]	GEANT4 v.8.0	SelectSeed	*WaterMC* vs. *CompleteMC*	3.0 –5.0		1.1			
Overall effect	This study	*egs_brachy* v2017.09.15	I25.S17plus	$D_{w,w\text{-}TG43}$ vs. $D_{m,m}$	4.1		2.0			
	Carrier et al.[6]	GEANT4 v.8.0	SelectSeed	*NoSeedMC* vs. *CompleteMC*	7.0		2.1			

Note: The water or prostate tissue phantoms are independent of MAR and TAS. This comparison is intended to verify the MC absorbed doses calculated in this study. MC-SUP, $D_{TG\text{-}43}$, and *NoSeedMC* are the TG-43-based MC absorbed dose calculations (neglect ISA and tissue composition). *Clinical* is the absorbed dose calculation with SPOT PRO TPS (Nucletron). LSKS is the line source MC simulation using TG-43 LS model. FMCS is the full MC simulation accounting only for ISA (excludes composition). *WaterMC* is the MC absorbed dose calculation in water accounting for ISA (excludes composition). *CompleteMC* is the most realistic MC calculation.
Abbreviations: DVH, dose–volume histogram; ISA, interseed scattering and attenuation; TPS, treatment planning system.

for D_{98}. They also reported a marginal overestimation of VariSeed v8.0 absorbed doses compared to MC superposition simulation MC-SUP for the 6711 seed using MCNPX v2.5.0 MC code. For the D_{90}, the relative difference between VariSeed and $D_{w,w\text{-}TG43}$ of 2.0% agrees with the 2.0% relative difference between VariSeed and $D_{TG\text{-}43}$ for the model 2301 source reported by Landry et al.[5] using GEANT4 v.9.3 MC code, where $D_{TG\text{-}43}$ is equivalent to $D_{w,w\text{-}TG43}$. The perfect agreement of D_{90} and V_{100} between the *Clinical* absorbed dose calculated with the SPOT PRO TPS (Nucletron) and TG-43-based MC calculation *NoSeedMC* in Carrier et al.[6] are in good agreement with this study. Carrier et al.[6] used SelectSeed and GEANT4 v.8.0 MC code.

3.2.3 | Interseed scattering and attenuation (ISA)

The VariSeed and $D_{w,w\text{-}MBDC}$ absorbed doses are calculated in the reference medium but the $D_{w,w\text{-}MBDC}$ MC simulation takes ISA into account. In Table 2, the computed dosimetry parameter results of VariSeed and $D_{w,w\text{-}TG43}$ are slightly higher than their $D_{w,w\text{-}MBDC}$ counterparts due to ISA. The maximum relative variations between VariSeed and $D_{w,w\text{-}MBDC}$ in the PTV are 4.4% and 5.8% for D_{98} and V_{150}, respectively. The relative differences for the OARs are 3.9% and 8.8% for the urethra and rectum, respectively. The MC absorbed dose verification for the contribution of ISA is shown in Table 3. The D_{90} and V_{100} overestimation by the TG-43 calculations of 1.8% and 0.51%, respectively, due to the absence of ISA in this study is in good agreement with the 2.0%–5.0% and 0.41% reported in Chibani et al.[2,34] The D_{90} in this study is, however, small compared to the 4.0% reported in Carrier et al.,[6] in which it was found that although ISA depends on the number of seeds per unit prostate volume n_{seed}, a high n_{seed} does not correspond automatically to a high number of small interseed distances because the seeds are not distributed homogeneously. Thus, implants with higher number of tightly clustered seeds will have a higher ISA contribution to the overall prostate absorbed dose even for cases with similar n_{seed}.[6] They exemplified their findings with two patients having similar n_{seeds} of 1.44 and 1.47 seeds cm^{-3} but different interseed attenuation on the D_{90} of −2.3% and −4.0%, respectively. The patient with −2.3% has 23 seed pairs with interseed distance less than 6 mm compared to the 44 seed pairs for the patient with −4.0%.[6]

In this study, 41 seeds are implanted in the prostate volume of 28.37 cm^3 giving a number of seeds per

TABLE 4 Comparison between the various Monte Carlo (MC) simulations give the percentage contribution of interseed scattering and attenuation (ISA) ($\Delta D_{w,w\text{-}TG43}$, $D_{w,w\text{-}MBDC}$), tissue composition ($\Delta D_{w,w\text{-}MBDC}$, $D_{m,m}$), and the combined effect of ISA and tissue composition ($\Delta D_{w,w\text{-}TG43}$, $D_{m,m}$)

	Prostate						Urethra	Rectum
	D_{50}	D_{90}	D_{98}	V_{75}	V_{100}	V_{150}	D_{10}	D_{2cc}
ISA (%)	1.4	1.8	2.0	0.1	0.5	3.1	0.9	1.6
Tissue composition (%)	1.9	2.4	2.9	0.2	1.5	3.9	2.3	7.0
Combined effect (%)	3.3	4.1	4.8	0.3	2.0	6.9	3.1	8.5
$\Delta D_{m,m}$, $D_{w,m}$ (%)	−0.8	−0.7	−0.3	−0.0	−0.4	−1.5	−0.7	3.5
$\Delta D_{w,w\text{-}TG43}$, $D_{w,m}$ (%)	2.5	3.5	4.5	0.3	1.7	5.5	2.4	11.7

Note: $\Delta D_{m,m}$, $D_{w,m}$ is the relative percentage differences of dose/volume between $D_{m,m}$ and $D_{w,m}$. $\Delta D_{w,w\text{-}TG43}$, $D_{w,m}$ is the relative percentage differences of dose/volume between $D_{w,w\text{-}TG43}$ and $D_{w,m}$.

unit prostate volume of 1.45 seeds cm^{-3}. The minimum and maximum distances between each seed pairs are 4.4 and 41.9 mm, respectively, with a mean distance of 22.4 mm between seed pairs. In this work, there is a total of two seed pairs with an interseed distance less than 6 mm compared to 23 and 44 seed pairs of Carrier et al.[6] As both studies have similar n_{seeds} of 1.45, 1.44, and 1.47 seeds cm^{-3}, the differences observed due to the ISA contribution of this study (1.8%) with respect to Carrier et al.[6] (4.0%) is due to a much lower number of tightly clustered seed pairs with interseed distance less than 6 mm in this study (only two seed pairs). The percentage contribution of ISA ($D_{ww\text{-}TG43}$ vs. $D_{w,w\text{-}MBDC}$) for all DVH parameters are presented in Table 4. ISA contributes 1.8% and 2.0% of D_{90} and D_{98}, respectively, with V_{150} having the maximum ISA contribution of 3.1% to the prostate. The OARs have an ISA contribution of 0.9% and 1.6% to the urethra and rectum, respectively.

3.2.4 | Tissue composition, $D_{m,m}$

The TG-186 patient phantom is used for the substantial MC simulations, $D_{m,m}$, where particles are transported in tissues and absorbed dose is scored in tissue, thus accounting for both ISA and tissue heterogeneities.[3]

According to Table 2, VariSeed overestimated the D_{90} and V_{100} parameters by 6.0% and 3.1%, respectively, compared to the more realistic MC simulation, $D_{m,m}$. These results agree with the D_{90} and V_{100} overestimation of 7.0% and 2.1%, respectively, between the *clinical* method (SPOT PRO TPS, Nucletron) and the *CompleteMC* method reported by Carrier et al.[6] as shown in Table 3. The *clinical* and *NoSeedMC* methods have the same absorbed dose distribution. This study shows a systematic decrease of 2.4% for the D_{90} parameter due to tissue composition and a global difference of 4.1% due to the combined effect of ISA (1.8%) and tissue composition (2.4%) as depicted in Tables 3 and 4. In Table 3, the decrease in D_{90} due to tissue composition in this study agrees with the 3.0%–5.0% reported by Carrier et al.[6,35] The combined effect of this study is lower than the 7.0% mean difference reported by Carrier et al.,[6] of which 4.0% and 3.0% are due to ISA and tissue composition, respectively.[3,6] The reduced combined effect is due to the small interseed attenuation contribution of this study discussed earlier. The voxelized patient phantoms used in Chibani et al.[2,34] and Carrier et al.[6,35] are built by stacking voxels in an ellipsoid and cube, respectively. These voxels are then given the densities of water and prostate for TG-43 and MBDC calculations, respectively. These phantoms and the one used in this work are independent of MAR and TAS. The relative percentage differences of ISA and tissue heterogeneity between this study and these published results by Chibani et al.,[2,34] Landry et al.,[5] Mason et al.,[33] and Carrier et al.[6,35] are mainly Type B uncertainties due to the different ^{125}I source models and MC codes.

3.2.5 | $D_{w,m}$ MC method

For $D_{w,m}$, particles are transported in tissues but absorbed dose is scored in water in accordance to the conventions of TG-186.[3] Although the TG-186 report only recommends reporting of $D_{m,m}$ as opposed to the competing $D_{w,m}$ when using MBDCAs, some MC researchers, however, used post-implant CT-based phantoms to calculate $D_{w,m}$. It is thus also important to investigate the dosimetric effects of MAR and TAS in these studies. For the D_{90} parameter, the relative difference between VariSeed and $D_{w,m}$ is 5.4% (Table 2) and between $D_{m,m}$ and $D_{w,m}$ is −0.7%, whereas the percentage deviation between $D_{w,w\text{-}TG43}$ and $D_{w,m}$ is 3.5%, as shown in Table 4.

3.2.6 | Comparison with post-implant CT-based phantom publications

Post-implant CT-based phantom studies applied MAR and TAS to mitigate metallic artifacts due to BT seeds and the tissue types of the voxelized patient phantoms are assigned using organ-specific materials or a CT

TABLE 5 Comparison between the Monte Carlo (MC) absorbed dose in this study and absorbed doses scored in post-implant CT-based phantoms from previous studies using different ^{125}I sources and MC codes

	Study	MC code	^{125}I source model	Compared MC doses	Relative difference of DVH parameters (%)					
					D_{90}	D_{98}	V_{100}	V_{150}	D_{10}	D_{2cc}
Tissue effect ($D_{m,m}$)	This study	*egs*_brachy v2017.09.15	I25.S17plus	$D_{w,w\text{-}MBDC}$ vs. $D_{m,m}$	2.4					
	Oliveira et al.[36]	MCNPX v.27a	Model 6711	HT vs. W	2.8–3.9					
Overall effect ($D_{m,m}$)	This study	*egs_brachy* v2017.09.15	I25.S17plus	$D_{w,w\text{-}TG43}$ vs. $D_{m,m}$	4.1	4.8	2.0	6.9	3.1	8.5
	Mason et al.[33]	MCNPX v2.5.0	Model 6711	MC-SUP vs. MC-CT-TISSUE	2.9	3.1	1.6	5.9	3.5	10.6
	Miksys et al.[8]	BrachyDOSE	SelectSeed model 125SL model LS-1 model 6711	**TG-43sim** vs. **MCref**	5.6	6.6* (D_{99})	2.4			5.2
Overall effect ($D_{w,m}$)	This study	*egs_brachy* v2017.09.15	I25.S17plus	$D_{w,w\text{-}TG43}$ vs. $D_{w,m}$	−3.5					
	Landry et al.[5]	GEANT4 v.9.3	Model 2301	$D_{TG\text{-}43}$ vs. $D_{w,m}$	−2.0					

Note: The post-implant CT-based phantoms applied MAR and TAS. This comparison is aimed at evaluating the dosimetric effects of MAR and TAS. HT is the calculation in the heterogeneous CT-patient phantom (neglects ISA). W is the calculations in water (neglects ISA). MC-SUP, **TG-43sim** is the TG-43 MC dose calculation (neglects ISA and tissue composition). MC-CT-TISSUE, **MCref** is the most realistic MC calculation.
Abbreviation: DVH, dose–volume histogram.

calibration curve. To evaluate the dosimetric effect of MAR and TAS, the computed MC absorbed doses of this work are compared to post-implant CT-based dosimetry calculations from previous MC studies using different ^{125}I source models and MC codes. The results of this comparison are shown Table 5.

Oliveira et al.[36] examined the effect of tissue heterogeneity for the model 6711 ^{125}I prostate implants in two patients using MCNPX v. 27a code. They reported a D_{90} overestimation of 2.8%–3.9% in the water calculations with respect to prostate tissue that agrees with the 2.4% recorded in this study.

Mason et al.[33] investigated the combined effect of ISA and tissue compositions in 30 patients treated with ^{125}I seeds model 6711 using MCNPX v2.5.0. MC-SUP and MC-CT-TISSUE where MC-SUP is the TG-43 calculation and MC-CT-TISSUE is MC absorbed dose calculated in a CT-based patient phantom. According to their calculations, the mean relative differences between MC-SUP and MC-CT-TISSUE for D_{90}, D_{98}, V_{100}, V_{150}, and D_{10} are 2.9%, 3.1%, 1.6%, 5.9%, and 3.5%, respectively. These results concur with the contribution of ISA and tissue composition to the global absorbed dose of 4.1%, 4.8%, 2.0%, 6.9%, and 3.1%, respectively, as documented in Table 5. They also reported a much higher relative difference of 10.6% for the rectum's D_{2cc} compared to the 8.5% recorded in this work.

Miksys et al.[8] retrospectively performed MC absorbed dose calculations with the EGSnrc-based MC code, BrachyDOSE for 613 patients who received ^{125}I permanent implant prostate BT using Nucletron SelectSeed, ProstaSeed 125SL, Draximage LS-1, and OncoSeed 6711 BT seeds. Similarly, the relative differences among TG-43 calculation, **TG-43sim**, and the most realistic MC calculation, **MCref**, are the combined effect of ISA and tissue composition. The average percentage difference between **TG-43sim** and **MCref** for D_{90} and V_{100} are 5.6% and 2.4%, respectively, and they are in good agreement with 4.1% and 2.0% recorded in this study, as shown in Table 5. For the rectum's D_{2cc}, the reported global absorbed dose differences of 5.2% agrees with the 8.5% documented in this study despite the fewer energetic particles reaching the rectum. Although they reported the prostate's D_{99} instead of D_{98}, the D_{99} of 6.6% is in concession with the D_{98} of 4.8% of this study.

To the best of our knowledge, Miksys et al.[8] described the largest MC dosimetric comparison between TG-43 and MBDCA methods for ^{125}I prostate BT with a very large cohort of 613 patients. The BrachyDOSE MC code used in their study and the *egs_brachy* MC code used in this work are both based on the EGSnrc MC system. This greatly reduces Type B uncertainties due to differences in MC code between their study and ours. They also used different ^{125}I sources, implying the reported mean absorbed doses is an average of Type B uncertainties of the various ^{125}I BT sources used in their study. The study of Miksys et al.[8] is thus the most favorable work to be compared with this study in order to evaluate the dosimetric effects of MAR and TAS on post-implant CT-based MC absorbed dose calculations for ^{125}I prostate implants. DVH absorbed dose metric parameters reported in the present work generally agree with such post-implant CT-based dosimetry studies.

Landry et al.[5] investigated the uncertainties of tissue composition in four patients treated with model 2301 ^{125}I BT source using GEANT4 v9.3 MC code. The $D_{w,m}$ is scored in a CT-based patient phantom, $MC_{\rho\,=\,CT}$. The $D_{TG\text{-}43}$ and $D_{w,m}$ simulations are, respectively, tantamount to $D_{w,w\text{-}TG43}$ and $D_{w,m}$ in this study. The reported mean relative difference of −2.0% for D_{90} is congruent with the −3.5% found in this study. The negative percentages imply that the TG-43 results are higher than $D_{w,m}$ values. Landry et al.[37] also compared $D_{w,m}$ and $D_{m,m}$ in four patients. The recorded mean $D_{90(w,m)}/D_{90(m,m)}$ ratio of 0.997 is in very good agreement with the calculated $D_{90(w,m)}/D_{90(m,m)}$ ratio of 1.007 in this study; where $D_{90(w,m)}$ and $D_{90(m,m)}$ are the D_{90} from the $D_{w,m}$ and $D_{m,m}$ MC calculations, respectively. The $D_{90(w,m)}/D_{90(m,m)}$ ratio is approximately unity because the prostate is almost water equivalent ($\rho = 1.04$ g cm^{-3}). Scoring in water ($D_{w,m}$) overestimates the prostate absorbed dose by less than 1% compared to scoring in prostate ($D_{m,m}$), as depicted in Table 4. Prostate with calcification will, however, give higher differences between $D_{m,m}$ and $D_{w,m}$ due to increased average density depending on the composition of the calcification.

3.3 | Study limitation

The major limitation of the study is the MC absorbed dose calculations for patients with visible calcification. The elemental composition and the mass density of the prostate/calcification mixture must be known and included as a tissue in the CT calibration curve used to generate realistic patient phantom. Different researchers used contrasting tissue densities for the same tissue. Mason et al.[33] reported an individual CT voxel density range of 1.30–2.38 g cm^{-3} for the prostate/calcification mixtures of 10 patients. Miksys et al.[8] used a CT density range of 1.14–1.27 g cm^{-3} for 50% prostate/50% calcification mixture and 2.0 g cm^{-3} instead of the recommended nominal density of 3.06 g cm^{-3} for the elemental composition of breast calcification.[3,34] The patient phantoms in these studies are derived by overwriting the CT voxels with the densities of the prostate/calcification mixture. As the CT-calibration curve in our study assigns tissues to voxels automatically, it may be difficult to obtain the percentages of the prostate and calcification in the generated TG-186 patient phantom. The correct mass-energy absorption coefficient for the elemental composition of prostate/calcification mixture is paramount for accurate MC absorbed dose calculations.

Mann-Krzisnik et al.[38] highlighted the need to update and unify the different elemental compositions of the irradiated tissues reported in the various literatures for more accurate MBDC calculations. They also noted the vast discrepancy of the elemental composition of prostate calcification used by various researchers. As MC absorbed dose calculations of low-energy BT sources are sensitive to elemental tissue composition, inadequate information on the elemental composition of homogeneous prostate/calcification mixtures, and the uncertainties of the published nominal densities used to derive CT number boundaries[3,7] makes it difficult to investigate the dosimetric effects of MAR and TAS on post-implant CT data with prostate/calcification mixtures in this work.

4 | CONCLUSIONS

This work has demonstrated as a proof of concept the possibility of performing MC absorbed dose calculations by virtually implanting seeds in a voxelized patient phantom derived from non-post-implant CT images of a patient. This study does not in any way demonstrate or advise that the implementation of MAR and TAS on post-implant CT images of patients should be sidestepped or evaded in routine clinical practice. The discrepancies observed between this work and post-implant CT-based dosimetry are largely Type B uncertainties due to differences in the ^{125}I source models and MC codes.

The implementation of MAR and TAS on post-implant CT images to mitigate metallic artifacts due to BT seeds and to assign tissue types to the voxelized patient phantom has no dosimetric effect on the MC absorbed dose calculations for ^{125}I permanent prostate implant.

ACKNOWLEDGMENT

We thank Dr. Marc J.P. Chamberland for *egs_brachy* technical support and the many insightful discussions.

Open Access funding enabled and organized by Projekt DEAL.

CONFLICT OF INTEREST

The authors have no conflicts of interest to disclose.

REFERENCES

1. Rivard MJ, Coursey BM, DeWerd LA, et al. Update of AAPM Task Group No. 43 Report: a revised AAPM protocol for brachytherapy dose calculations. *Med Phys*. 2004;31(3):633-674.
2. Chibani O, Williamson JF, Todor D. Dosimetric effects of seed anisotropy and interseed attenuation for 103Pd and 125I prostate implants. *Med Phys*. 2005;32(8):2557-2566.
3. Beaulieu L, Tedgren AC, Carrier JF, et al. Report of the Task Group 186 on model-based dose calculation methods in brachytherapy beyond the TG-43 formalism: current status and recommendations for clinical implementation. *Med Phys*. 2012;39(10):6208-6236.
4. DeMarco JJ, Smathers JB, Burnison CM, Ncube QK, Solberg TD. CT-based dosimetry calculations for 125I prostate implants. *Int J Radiat Oncol Biol Phys*. 1999;45(5):1347-1353.
5. Landry G, Reniers B, Murrer L, et al. Sensitivity of low energy brachytherapy Monte Carlo dose calculations to uncertainties in human tissue composition. *Med Phys*. 2010;37(10):5188-5198.

6. Carrier JF, D'Amours M, Verhaegen F, et al. Postimplant dosimetry using a Monte Carlo dose calculation engine: a new clinical standard. *Int J Radiat Oncol Biol Phys*. 2007;68(4):1190-1198.
7. Miksys N, Xu C, Beaulieu L, Thomson RM. Development of virtual patient models for permanent implant brachytherapy Monte Carlo dose calculations: interdependence of CT image artifact mitigation and tissue assignment. *Phys Med Biol*. 2015;60(15):6039-6062.
8. Miksys N, Vigneault E, Martin AG, Beaulieu L, Thomson RM. Large-scale retrospective Monte Carlo dosimetric study for permanent implant prostate brachytherapy. *Int J Radiat Oncol Biol Phys*. 2017;97(3):606-615.
9. Kawrakow I, Mainegra-Hing E, Rogers DWO, Tessier F, Walters BRB. *The EGSnrc Code System: Monte Carlo simulation of electron and photon transport. Technical Report PIRS-701*. National Research Council Canada; 2017.
10. Chamberland MJP, Taylor REP, Rogers DWO, Thomson RM. egs_brachy: a versatile and fast Monte Carlo code for brachytherapy. *Phys Med Biol*. 2016;61(23):8214-8231.
11. Low DA, Dempsey JF. Evaluation of the gamma dose distribution comparison method. *Med Phys*. 2003;30(9):2455-2464.
12. Pantelis E, Papagiannis P, Anagnostopoulos G, Baltas D. New 125 I brachytherapy source IsoSeed I25.S17plus: Monte Carlo dosimetry simulation and comparison to sources of similar design. *J Contemp Brachytherapy*. 2013;5(4):240-249.
13. Moutsatsos A, Pantelis E, Papagiannis P, Baltas D. Experimental determination of the Task Group-43 dosimetric parameters of the new I25.S17plus 125I brachytherapy source. *Brachytherapy*. 2014;13(6):618-628.
14. Carleton laboratory for radiotherapy physics TG-43 parameter database V2. Nov 2021. https://physics.carleton.ca/clrp/egs_brachy/seed_database/I125/BEBIG_I125.S17_plus
15. Thomson RM, Taylor REP, Chamberland MJP, Rogers DWO. *User Manual for egs_brachy. Report CLRP-17-02*. Carleton University Canada; 2017.
16. Taylor REP, Yegin G, Rogers DWO. Benchmarking BrachyDose: voxel-based EGSnrc Monte Carlo calculations of TG-43 dosimetry parameters. *Med Phys*. 2007;34(2):445-457.
17. Safigholi H, Chamberland MJP, Taylor REP, et al. Update of the CLRP TG-43 parameter database for LDR low-energy brachytherapy sources. *Med phys*. 2020;47(9):4656-4669.
18. Valdes-Cortez C, Mansour I, Rivard MJ, et al. A study of Type B uncertainties associated with photoelectric effect in low-energy Monte Carlo simulations. *Phys Med Biol*. 2021;66(10):105014.
19. Kawrakow I, Mainegra-Hing E, Tessier F, Townson R, Walters BRB. *The EGSnrc C++ Class Library. Technical Report PIRS-898*. National Research Council Canada; 2018.
20. *A Handbook of Radioactivity Measurements Procedures*. NCRP Publications; 1985. NCRP Report 58
21. Berger MJ, Hubbell JH. *XCOM: Photon Cross Sections on a Personal Computer*. NIST; 1987. Report NBSIR87-3597.
22. Kawrakow I. Electron impact ionization cross sections for EGSnrc. *Med Phys*. 2002;29:1230. abstract.
23. Rivard MJ, Ballester F, Butler WM, et al. Supplement 2 for the 2004 update of the AAPM Task Group No. 43 report: joint recommendations by the AAPM and GEC-ESTRO. *Med Phys*. 2017;44:e297-e338.
24. Walters B, Kawrakow I, Rogers DWO. *DOSXYZnrc User's Manual. NRCC Report PIRS-794revB*. National Research Council of Canada; 2018.
25. International Commission on Radiation Units and Measurements. *Photon, Electron, Proton and Neutron Interaction Data for Body Tissues. Report No. 46*. ICRU Publications; 1992.
26. Salembier C, Lavagnini P, Nickers P, et al. Tumour and target volumes in permanent prostate brachytherapy: a supplement to the ESTRO/EAU/EORTC recommendations on prostate brachytherapy. *Radiother Oncol*. 2007;83(1):3-10.
27. Deasy JO, Blanco AI, Clark VH. CERR: a computational environment for radiotherapy research. *Med Phys*. 2003;30(5):979-985.
28. Ezzell GA, Burmeister JW, Dogan N, et al. IMRT commissioning: multiple institution planning and dosimetry comparisons, a report from AAPM Task Group 119. *Med Phys*. 2009;36(11):5359-5373.
29. Yang Y, Rivard MJ. Comparison of brachytherapy dose distributions using the gamma-index method. Joint AAPM/COMP meeting. 2011. abstract.
30. Heilemann G, Poppe B, Laub W. On the sensitivity of common gamma-index evaluation methods to MLC misalignments in Rapidarc quality assurance. *Med Phys*. 2013;40(3):031702.
31. Fredh A, Scherman JB, Fog LS, et al. Patient QA systems for rotational radiation therapy: a comparative experimental study with intentional errors. *Med Phys*. 2013;40(3):031716.
32. Mason J, Al-Qaisieh B, Bownes P, Henry A, Thwaites D. Monte Carlo investigation of I-125 interseed attenuation for standard and thinner seeds in prostate brachytherapy with phantom validation using a MOSFET. *Med Phys*. 2013;40(3):031717-031728.
33. Mason J, Al-Qaisieh B, Bownes P, Henry A, Thwaites D. Investigation of interseed attenuation and tissue composition effects in 125I seed implant prostate brachytherapy. *Brachytherapy*. 2014;13(6):603-610.
34. Chibani O, Williamson JF. MCPI: a sub-minute Monte Carlo dose calculation engine for prostate implants. *Med Phys*. 2005;32(12):3688-3698.
35. Carrier JF, Beaulieu L, Therriault-Proulx F, Roy R. Impact of interseed attenuation and tissue composition for permanent prostate implants. *Med Phys*. 2006;33(3):595-604.
36. Oliveira SM, Teixeira NJ, Fernandes L, Teles P, Vaz P. Dosimetric effect of tissue heterogeneity for 125I prostate implants. *Rep Pract Oncol Radiother*. 2014;19(6):392-398.
37. Landry G, Reniers B, Pignol JP, Beaulieu L, Verhaegen F. The difference of scoring dose to water or tissues in Monte Carlo dose calculations for low energy brachytherapy photon sources. *Med Phys*. 2011;38(3):1526-1533.
38. Mann-Krzisnik D, Verhaegen F, Enger SA. The influence of tissue composition uncertainty on dose distributions in brachytherapy. *Radiother Oncol*. 2018;126(3):394-410.

SUPPORTING INFORMATION

Additional supporting information can be found online in the Supporting Information section at the end of this article.

How to cite this article: Assam I, Vijande J, Ballester F, Pérez-Calatayud J, Poppe B, Siebert F-A. Evaluation of dosimetric effects of metallic artifact reduction and tissue assignment on Monte Carlo dose calculations for ^{125}I prostate implants. *Med Phys*. 2022;49:6195–6208. https://doi.org/10.1002/mp.15865